International Current Journal of Engineering and Science
Volume 5, Issue 11, pp 19-23, November 2026
ISSN (Online): 2583-7257
Article DOI: doi.org/10.47001/ICJES/2026.511003

Finite Element Stress and Strain Analysis of a Cogged Chloroprene Rubber V-Belt in a Turbine Cooling Air Unit

[1]Toni Prahasto, [2]*Ojo Kurdi, [3]Dwi Basuki Wibowo, [4]Achmad Chairil Isthafat

[1,2,3,4]Departement of Mechanical Engineering, Faculty of Engineering, Universitas Diponegoro, Semarang, Indonesia
*Corresponding Author's E-mail: ojokurdi@ft.undip.ac.id

Abstract **- The Turbine Cooling Air cooler plays a vital role in maintaining operational reliability in power generation systems by reducing the temperature of compressed bleed air prior to entering the turbine rotor. Cogged V-belt drive was used to be a power transmission in this cooling unit by connecting the electric motor to the cooling fan, where excessive cyclic tensile and bending loads can induce localized fatigue cracking and premature structural failure. This study investigates the internal stress and strain distributions of a cogged Chloroprene Rubber V-belt using a non-linear three-dimensional finite element method in ANSYS Static Structural. A representative volume element submodel with a length of thirty-two millimeters comprising three cogs was constructed to eliminate boundary cut artifacts and ensure numerical convergence. The hyperelastic behavior of Chloroprene Rubber was modeled using a two-parameter Mooney-Rivlin constitutive formulation fitted from uniaxial, biaxial, and planar shear experimental data. Under a displacement-controlled longitudinal extension of fifteen millimeters applied via a remote displacement boundary condition, the simulation yielded a maximum total deformation of 15.217 millimeters. The maximum principal elastic strain reached 0.6922 and was heavily concentrated at the tooth root fillets, particularly on the middle cog, identifying the tooth root as the primary hotspot for fatigue crack initiation. Furthermore, the maximum equivalent von Mises stress and maximum principal stress were recorded at 5.343 megapascals and 5.8328 megapascals, respectively, remaining within safe material limits. These findings provide a targeted visual inspection reference for preventive maintenance of industrial V-belt drives.**

Keywords: Finite Element Method, Cogged V-Belt, Turbine Cooling Air Cooler, Chloroprene Rubber, Mooney-Rivlin Model, Von Mises Stress, Hyperelastic Material, Static Structural Analysis.

I. INTRODUCTION

Industrial power generation systems rely on auxiliary cooling subsystems to preserve thermal efficiency and mechanical integrity during continuous operation. Among these subsystems, the Turbine Cooling Air (TCA) cooler functions as a critical heat exchanger that lowers the temperature of high-pressure bleed air extracted from the compressor—typically reducing air temperatures from approximately 442.6°C to 217.9°C—before routing it to cool rotating turbine components [1]. In many combined thermal cycles, the TCA cooler is arranged in series with a fuel gas heater to optimize waste heat recovery [1]. The forced-convection cooling fan inside a TCA cooler unit is commonly driven by a V-belt transmission mechanism coupled to an electric motor, valued for its compact layout, vibration damping, low operational noise, and high traction capacity generated by the wedging action between the trapezoidal belt flanks and pulley grooves [2], [3].

Maintaining the structural reliability of V-belt drives is essential to prevent unscheduled downtime in continuous 24-hour power plant operations [4]. Operational belt tension directly governs transmission performance: insufficient tension induces belt-pulley slip and power loss, whereas excessive tension and repeated bending around small-diameter pulleys accelerate material fatigue and flexural cracking [5], [6]. Prolonged cyclic loading under elevated ambient temperatures can further promote polymer aging, surface hardening, and brittle fracture [7]. Consequently, mapping internal stress and strain distributions is critical for condition-based maintenance, as localized high-stress regions pinpoint the exact sites of crack initiation [5].

Conventional analytical belt formulas estimate macroscopic tension and nominal service life, yet they cannot resolve localized three-dimensional stress concentrations across complex cogged geometries. The Finite Element Method (FEM) overcomes this limitation by capturing non-linear hyperelastic material responses and geometric discontinuities [6], [8], [9]. Previous numerical investigations have demonstrated that finite element modeling of elastomeric

© 2026 ICJES All Rights Reserved

International Current Journal of Engineering and Science
Volume 5, Issue 11, pp 19-23, November 2026
ISSN (Online): 2583-7257
Article DOI: doi.org/10.47001/ICJES/2026.511003

belts accurately predicts flexural fatigue hotspots and deformation behavior under multi-axial loading [6], [10]. Therefore, this study employs a non-linear three-dimensional static structural finite element simulation to evaluate the deformation, principal elastic strain, von Mises stress, and principal stress distributions of a cogged Chloroprene Rubber V-belt used in a TCA cooler unit, establishing an engineering basis for targeted preventive maintenance.

II. METHODOLOGY

2.1 Geometrical Modeling and Representative Submodel

The analyzed component is a cogged V-belt (type BX77) utilized in a three-groove pulley drive system of a TCA cooler unit driven by an 11.2 kW electric motor operating up to 1,500 rpm. The standard cross-sectional geometry of the belt features a top width of 16.5 mm, a thickness of 11.0 mm, an included groove angle of 38°, and a pitch length of 77 in(1,955.8 mm).

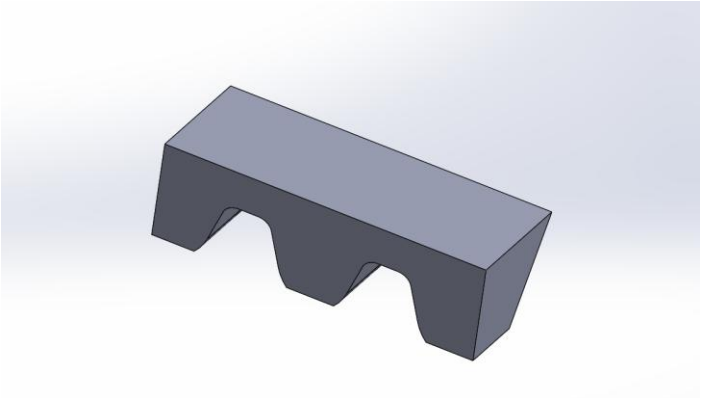


Figure 1: Geometrical Modelling

2.2 Hyperelastic Material Characterization

The belt body was modeled as a homogeneous, isotropic, incompressible hyperelastic elastomer composed of Chloroprene Rubber (CR), omitting internal reinforcement cords to focus on matrix strain localization. Unlike linear elastic metals governed by Hooke's law, Chloroprene Rubber exhibits highly non-linear stress-strain behavior under large deformations. To capture this response, the two-parameter Mooney-Rivlin constitutive model was adopted [11]. For an incompressible hyperelastic material, the strain energy density function W_d is expressed in terms of the first and second invariants (I_1 and I_2) of the right Cauchy-Green deformation tensor [11], where C_{10} and C_{01} are empirically determined material constants. Under uniaxial tension, the nominal stress-strain relationship is defined as:

Experimental stress-strain datasets from uniaxial, biaxial, and planar shear tests of Chloroprene Rubber [12] were imported into the ANSYS Engineering Data module to perform non-linear curve fitting. The resulting fitted constants and physical properties applied in the simulation are summarized in Table 1.

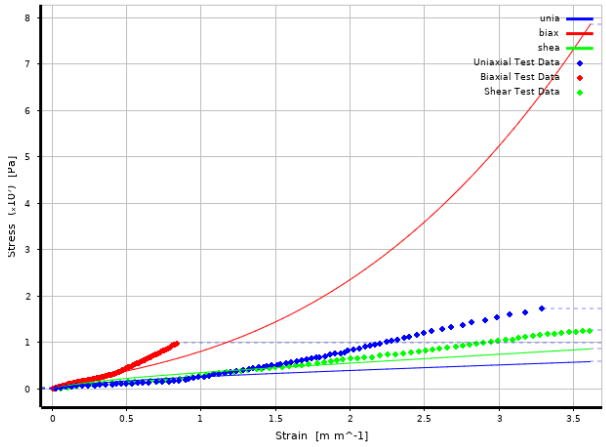


Figure 2: Hyperelastic curve fitting of uniaxial, biaxial, and shear test data using the two-parameter Mooney-Rivlin model

Table 1: Material properties of Chloroprene Rubber used in the finite element simulation

Parameter	Value
Density	1250 kg/m^3
Konstanta C10	0.5622 Mpa
Konstanta C01	0.3743 Mpa

2.3 Finite Element Discretization and Boundary Conditions

The 3D submodel was imported into ANSYS Workbench and solved using the Static Structural module under constant room temperature assumptions. To prevent element lock-up during large hyperelastic deflections, the physics preference was configured to *Nonlinear Mechanical* with *Quadratic* element order. Domain discretization utilized a global element size of 2.0 mm refined with a 1.0 mm body sizing to accurately resolve steep strain gradients along the cog tooth roots. A *Sweep Method* was applied along the 32 mm extrusion axis to generate structured hexahedral and prismatic elements. The final mesh comprised 3,432 elements and 16,511 nodes, achieving a maximum skewness of 0.46097 and an average skewness of 0.18519, which falls well within the recommended threshold (<0.50) for non-linear finite element accuracy.

© 2026 ICJES All Rights Reserved

International Current Journal of Engineering and Science
Volume 5, Issue 11, pp 19-23, November 2026
ISSN (Online): 2583-7257
Article DOI: doi.org/10.47001/ICJES/2026.511003

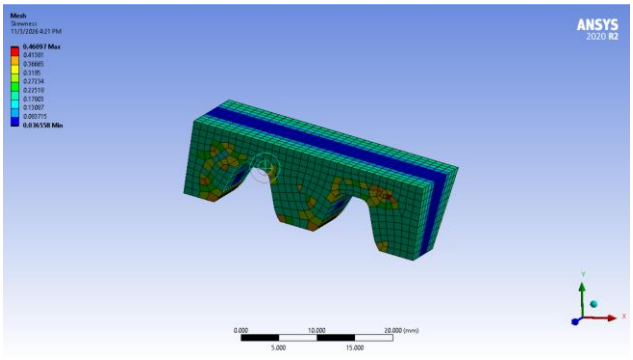


Figure 3: Discretized finite element mesh and skewness quality distribution of the V-belt submodel

Because force-controlled loading on highly flexible hyperelastic elastomers frequently induces excessive element distortion and Newton-Raphson solver divergence, a displacement-controlled loading scheme was implemented. One cut cross-section of the 32 mm segment was fully constrained using a *Fixed Support*, while the opposite cut face was subjected to an axial *Remote Displacement* of $\Delta x = 15$ mm along the longitudinal X-axis. This extension corresponds to a nominal axial strain of 46.87%, representing the combined tensile and flexural strain state experienced when bending around the smaller pulley. Using a *Remote Displacement* pilot node permits natural cross-sectional rotation and lateral contraction, eliminating artificial stiffness locking and spurious edge stress concentrations.

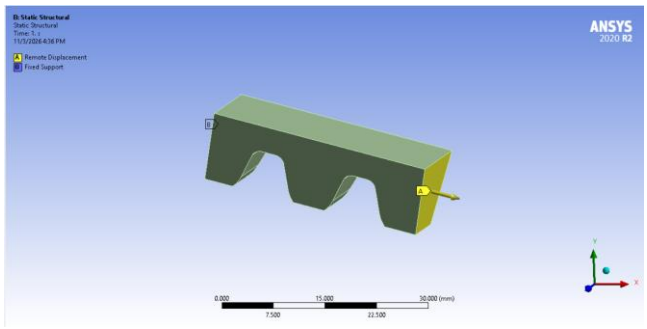


Figure 4: Boundary conditions applied in ANSYS Static Structural showing the Fixed Support and 15 mm longitudinal Remote Displacement

III. RESULTS AND DISCUSSIONS

3.1 Total Deformation Analysis

The total deformation contour ($\delta_{\text{total}} = \sqrt{\delta_x^2 + \delta_y^2 + \delta_z^2}$) across the 32 mm V-belt segment exhibits a smooth, continuous displacement gradient progressing from 0 mm at the fixed end to a maximum of 15.217 mm at the loaded end. The peak resultant displacement slightly exceeds the prescribed 15 mm longitudinal input by 0.217 mm due to transverse Poisson contraction and cross-sectional necking inherent to incompressible elastomeric deformation. The absence of abrupt contour discontinuities confirms numerical stability and element integrity throughout the non-linear solution steps.

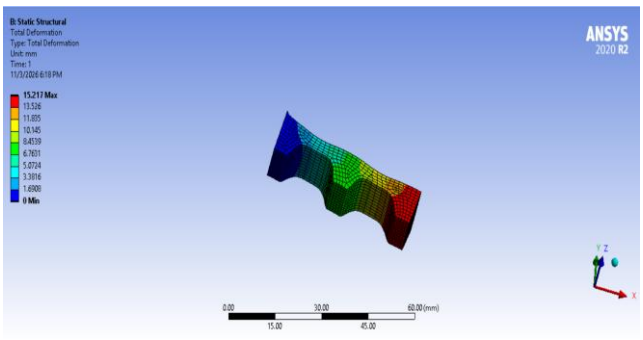


Figure 5: Contour distribution of total deformation under 15 mm longitudinal extension

3.2 Von Mises and Maximum Principal Stress Analysis

To assess structural integrity against material failure, equivalent (von Mises) stress (σ_{VM}) and maximum principal stress (σ_1) distributions were extracted. The von Mises stress reaches a maximum of 5.343 Mpa and a minimum of 0.020517 Mpa, concentrating along the upper back section of the belt and the adjacent tooth root fillets. This distribution reflects the coupled effect of direct axial tension and localized bending induced as the cogged profile stretches.

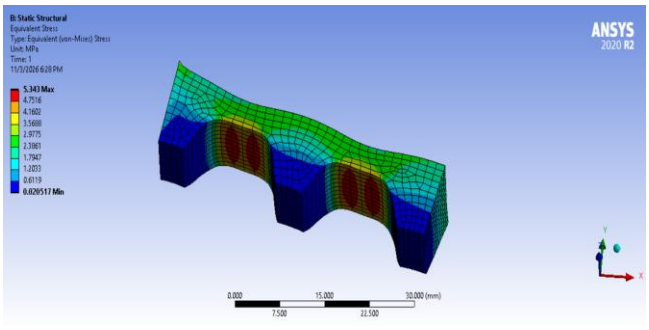


Figure 6: Equivalent (von Mises) stress distribution across the cogged V-belt submodel

Similarly, the maximum principal stress reaches a peak tensile value of 5.8328 Mpa on the upper flat surface of the belt and a minimum value of -0.018328 Mpa near the lower cog tips. The minor negative stress indicates localized micro-compression generated by transverse deformation of the cogs. Both the peak von Mises stress(5.343 Mpa) and peak principal tensile stress 5.8328 Mparemain well below the ultimate tensile strength of Chloroprene Rubber, demonstrating that the belt sustains extreme localized elongation without instantaneous static rupture.

© 2026 ICJES All Rights Reserved

International Current Journal of Engineering and Science
Volume 5, Issue 11, pp 19-23, November 2026
ISSN (Online): 2583-7257
Article DOI: doi.org/10.47001/ICJES/2026.511003

3.3 Maximum Principal Elastic Strain and Critical Hotspot Identification

Evaluating the maximum principal elastic strain (ε_{max}) reveals the exact regions susceptible to cyclic fatigue crack initiation. Under the 15 mm extension, the simulation recorded a peak principal elastic strain of 0.6922 (69.22%) and a minimum of 0.007652. As illustrated in Figure 6, high-strain zones are sharply localized at the curved tooth root fillets along the underside of the belt. The geometric transition at each tooth root acts as a natural stress-strain riser (notch effect) under tensile elongation. Crucially, the middle cog exhibits a clean, symmetric strain concentration free from boundary end-effects, confirming the tooth root fillet as the primary structural hotspot where micro-cracks initiate during continuous operation. Table 2 summarizes the quantitative finite element outputs.

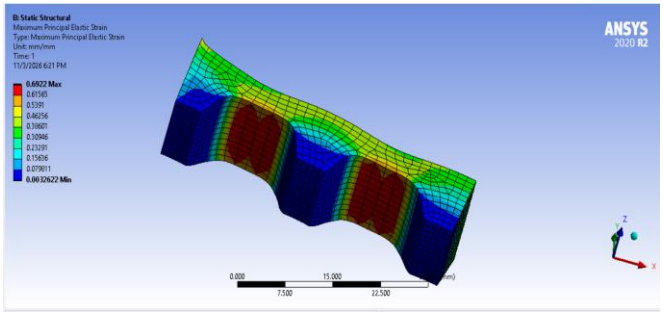


Figure 7: Distribution of maximum principal elastic strain highlighting peak strain localization at the middle tooth root

Table 2: Summary of non-linear static structural finite element simulation results

Output	Min Value	Max Value	Unit	Location
Total Def.	0	15.217	mm	Loaded cross-section edge
Max Principal Strain	0.007652	0.6922	mm/mm	Middle cog tooth root fillet
Von Misses	0.020517	5.343	Mpa	Upper belt back and tooth root
Max Principal Stress	-0.018328	5.8328	Mpa	Upper belt surface (tension)

From an operational maintenance standpoint, while the stress magnitudes confirm static safety, the severe strain amplification at the tooth roots (69.22%local principal strain versus 46.87% nominal axial strain) explains why cogged V-belts predominantly fail via root cracking. Maintenance personnel overseeing TCA cooler units should therefore prioritize close visual inspection of the inner cog root fillets for early signs of crazing, rubber hardening, or transverse micro-cracks during scheduled shutdowns.

IV. CONCLUSION

A three-dimensional non-linear finite element analysis was successfully conducted to evaluate the mechanical response of a cogged Chloroprene Rubber V-belt used in a Turbine Cooling Air cooler unit. Utilizing a 32 mm three-cog submodel with a two-parameter Mooney-Rivlin hyperelastic material formulation under a 15 mm longitudinal remote displacement, the simulation yielded a continuous total deformation peaking at 15.217 mm. The maximum principal elastic strain reached 0.6922 (69.22%) and was concentrated specifically at the middle tooth root fillets, establishing this region as the primary hotspot for fatigue crack initiation. Meanwhile, the maximum equivalent von Mises stress of 5.343 Mpaand maximum principal tensile stress of 5.8328 Mparemained safely within the ultimate strength limits of Chloroprene Rubber. These findings provide maintenance engineers with a clear physical reference to focus routine visual inspections on the cog root areas to prevent unexpected belt failure. Future investigations should incorporate thermal-structural coupling to account for elevated ambient operating temperatures and thermal aging effects on elastomer durability.

ACKNOWLEDGEMENT

The authors gratefully acknowledge the Department of Mechanical Engineering, Faculty of Engineering, Universitas Diponegoro, for providing the computational facilities and academic support required to complete this study.

REFERENCES

[1] Yang, C., Yin, Q., Xiao, R., Xue, Z., & Ma, X. (2025). Waste-heat utilization for turbine air cooler and fuel heater in gas turbine combined cycle. *Applied Thermal Engineering*, 277. https://doi.org/10.1016/j.applthermaleng.2025.127061.

[2] Amanov *et al.* (2019). A. Amanov *et al.*, "Experimental Investigation on Friction and Wear Behavior of the Vertical Spindle and V-belt of a Cotton Picker," *Materials*, vol. 12, no. 5, p. 773, 2019. doi: 10.3390/ma12050773.

[3] Yu, Z., Cui, Y., Zhang, Q., Liu, J., & Qin, Y. (2022). Thermo-mechanical coupled analysis of V-belt drive

© 2026 ICJES All Rights Reserved

International Current Journal of Engineering and Science
Volume 5, Issue 11, pp 19-23, November 2026
ISSN (Online): 2583-7257
Article DOI: doi.org/10.47001/ICJES/2026.511003

system via absolute nodal coordinate formulation. *Mechanism and Machine Theory*, 174. https://doi.org/10.1016/j.mechmachtheory.2022.104906 .

[4] Omorodion *et al.* (2020) I. Omorodion *et al.*, "Effect of under belting a multiple V-belt drive," *Journal of Advances in Science and Engineering*, vol. 3, no. 1, 2020. doi: 10.37121/jase.v3i1.72.

[5] Mascenik, J., & Coranic, T. (2024). The Influence of Changing Belt Loading Conditions on the Operational Condition of the Belt Transmission. *Actuators*, 13(12). https://doi.org/10.3390/act13120506.

[6] Li, W., & Xin, Z. (2018). Flexural fatigue life prediction of a tooth V-belt made of fiber reinforced rubber. *International Journal of Fatigue*, 111, 269–277. https://doi.org/10.1016/j.ijfatigue.2018.02.025.

[7] Xu, B., Liu, Y., Wang, Y., Ni, X., & Wang, X. (2021). Advanced calculation model of V-belt temperature field. *ElektronikaIr Elektrotechnika*, 27(3), 4–14. https://doi.org/10.5755/j02.eie.29003.

[8] Chen H.Y., Hu X.B., Zhu H.D., et al., 2020, Analysis of internal stress distribution characteristics of conveyor belt, *Machine Design*, 37, 4, 55-60.

[9] Hoover, D., & Kumar, A. V. (2022). Immersed boundary Mindlin-Reissner 3D shell element for modeling isotropic and laminated composite shells. *Finite Elements in Analysis and Design*, 208. https://doi.org/10.1016/j.finel.2022.103794

[10] Liu, J., Zheng, J. yun, Ma, K., Fu, B., Chen, S., & Zhao, Y. (2023). Stress analysis and wear life prediction of metal sheet of CVT under high speed condition. https://doi.org/10.21203/rs.3.rs-1663832/v1.

[11] Yao, Q., Dong, P., Zhao, Z., Li, Z., Wei, T., Wu, J., Qiu, J., & Li, W. (2023). Temperature dependent tensile fracture strength model of rubber materials based on Mooney-Rivlin model. *Engineering Fracture Mechanics*, 292. https://doi.org/10.1016/j.engfracmech.2023.109646.

[12] Kim, B., Lee, S. B., Lee, J., Cho, S., Park, H., Yeom, S., & Park, S. H. (2012). A comparison among Neo-Hookean model, Mooney-Rivlin model, and Ogden model for Chloroprene rubber. *International Journal of Precision Engineering and Manufacturing*, 13(5), 759–764. https://doi.org/10.1007/s12541-012-0099-y

Citation of this Article:

Toni Prahasto, Ojo Kurdi, Dwi Basuki Wibowo, & Achmad Chairil Isthafat. (2026). Finite Element Stress and Strain Analysis of a Cogged Chloroprene Rubber V-Belt in a Turbine Cooling Air Unit. *International Current Journal of Engineering and Science (ICJES)*, 5(11), 19-23. Article DOI: https://doi.org/10.47001/ICJES/2026.511003

****

© 2026 ICJES All Rights Reserved